Chapter 6

Electrons in the Cylindrical Trap

The non-destructive detection techniques outlined in Chapter 5 are used to observe electrons in the new open endcap Penning trap. Electrons are generated by the field emitting point, and guided to the degrader (see Fig. 5.5) at the far end of the trap by the 5.9 T magnetic field. Low energy secondary electrons from the degrader surface travel back through the harmonic potential region. A small reduction of energy (via collisions or coupling to the cyclotron motion which rapidly cools by synchrotron radiation) is sufficient for the electrons to become bound in the harmonic well.

6.1 Observing the Axial Motion

6.1.1 Damping Rates and Electron Number

Electrons loaded in the harmonic well can be observed using the signal from the detection circuit tuned on resonance with the electron axial frequency $\nu_z(e^-)$. The axial motion is coupled to a resistor, damping this motion with a time constant of $\tau_z \approx 0.3$ seconds for a single electron.

The electron cyclotron motion ($\nu_c' \approx 164$ GHz at 5.9 T) damps by synchrotron radiation to the 4K environment. The radiation damping rate is

$$\frac{dE}{dt} = -\gamma_c E, \tag{6.1}$$

where

$$\gamma_c = \frac{4}{3c}\left(\frac{e^2}{mc^2}\right)\omega_c^2. \tag{6.2}$$

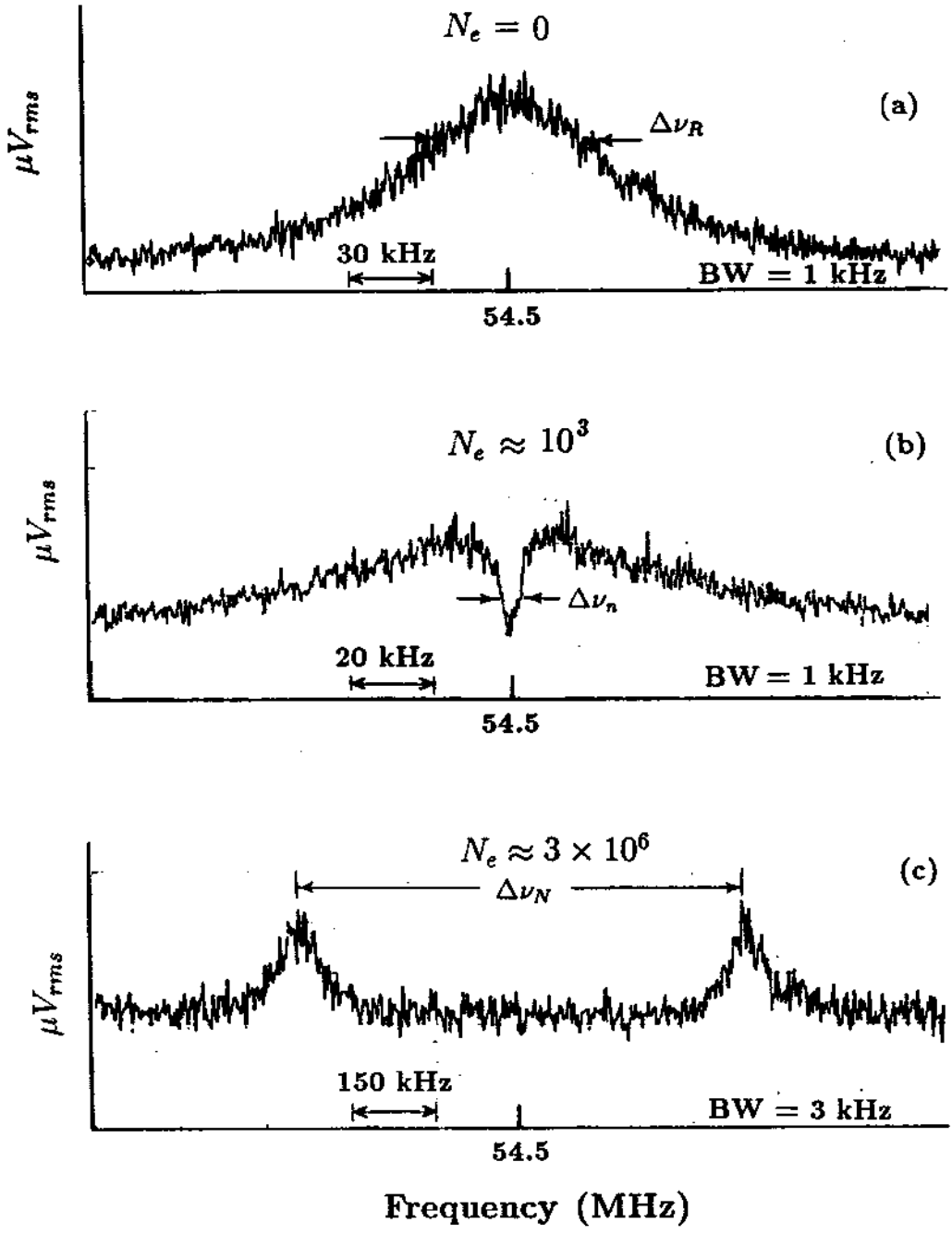

Figure 6.1: Voltage induced across the axial detection circuit with (a) no electrons loaded, (b) a small number of confined electrons, and (c) a large number of confined electrons.

For an electron with $\nu_c' \approx 164$ GHz, $\gamma_c^{-1} \approx 0.08$ seconds the rate is proportional to $1/\mathrm{m}^3$ so that the energy loss by this mechanism for a particle as massive as the proton would be insignificant at the existing trapping fields.

The effect of electrons on the noise spectra of the axial detection circuit is shown in Fig. 6.1. Figure 6.1(a) shows a noise spectra with no electrons in the trap. In Fig. 6.1(b) and (c), electrons are tuned to the same frequency as the noise spectra in Fig. 6.1(a). An interpretation of such signals has been given by Wineland and Dehmelt [115]. The axial motion of a confined electron can be modeled as a series resonant lc circuit (with $l = md^2/e^2$ and $c = [(2\pi\nu_z)^2 l)]^{-1}$ in parallel with the detection LCR circuit. For sufficiently small numbers of electrons (when $(\omega l_1/n)/R \gg R\omega C$) the model can be generalized to n electrons by scaling $l \rightarrow l_1/n$ and $c \rightarrow nc_1$. An observable dip results from the series lc circuit shorting the LCR circuit on resonance at $2\pi\nu_z = 1/\sqrt{lc}$. The measured dip width $\Delta\nu_n$ gives the particle number by

$$n = 2\pi l_1 \frac{\Delta\nu_n}{R} = \frac{\Delta\nu_n}{\Delta\nu_1}. \tag{6.3}$$

The parallel resistance R of the LCR circuit is determined from the width of the measured noise spectra ν_{NR}. Using Eq. 6.3 and the single linewidth $\Delta\nu_1$ from Table 5.1, the number of electrons in Fig. 6.1(b) is about 1000.

For much larger numbers (when $(\omega l_1/N)/R \ll R\omega C$), the spectra shown in Fig. 6.1(c) is observed. The coupling between the lc and LC circuits is dependent on particle number. For sufficiently large numbers, the response frequencies split. The splitting $\Delta\nu_N$ is related to the confined number by

$$N = (2\pi\Delta\nu_N)^2 l_1 C = \frac{(\Delta\nu_N)^2}{\Delta\nu_1 \Delta\nu_{NR}} \tag{6.4}$$

where $\Delta\nu_N$ is measured from peak to peak, and C is given in Table 5.1. For the case shown in Fig. 6.1(c), approximately 3×10^6 electrons are stored in the trap with a density of order $10^7/cm^3$. The signal in Fig. 6.1(c) provides a measure of the number of electrons in the large clouds used for electron cooling antiprotons.

As a check, to determine electron number we have quickly removed the trapping potential on the harmonic well and directly collected and integrated the electrons

as they struck the degrader. Doing this we find agreement with the non-destructive linewidth determinations to better than a factor of 2.

6.1.2 Phase Sensitive Detection and Locking the Axial Motion

Using a small number of electrons such as shown in Fig. 6.1(b), we can obtain phase information of the oscillating center of mass axial motion. The electrons are driven with an external frequency source applied to the lower endcap as shown in Fig. 5.5. In practice, since the direct feedthrough of such a drive would saturate the sensitive detection preamplifier, the trap voltage is modulated at ν_{mod} producing FM sidebands on the particle resonant frequency of $\nu_z \pm \nu_{mod}$. We typically modulate the ring potential for electrons at $\nu_{mod}/\nu_z \approx 0.02$. The axial motion is driven on $\nu_z \pm \nu_{mod}$ leaving the detection region at ν_z far from the direct feedthrough.

The detected axial signal at $\nu_z \approx 54.5$MHz is mixed down with the axial drive at $\nu_z + \nu_{mod} \approx 55.7$ MHz using a double balanced mixer. The mixed signal near 1.2 MHz, goes to the input of a EG&G PAR model #5202 Lock-in amplifier with the reference being the modulating drive at ν_{mod}. The resulting Lorentzian lineshapes are well understood [13].

The shape of these coherent responses depends on the degree to which the trap is harmonic. For a trap with anharmonic components added (for example by adjusting the compensation ratio V_c/V_0), the response becomes that of an anharmonic oscillator. By observing the absorption lineshape as a function of changing the ratio V_c/V_0, the trap harmonicity can be optimized.

With the dispersion curve, the zero crossing serves as a sensitive error signal to lock the axial frequency to the external oscillator used to drive the axial motion. The frequency is held at the zero crossing by feeding back a voltage to the trap endcaps. By monitoring the feedback voltage, we observe changes or perturbations that would cause a shift $\Delta\nu_z$, but are compensated by the feedback circuit. Such shifts are easily calibrated by introducing a known change in the drive frequency and measuring the correction signal.

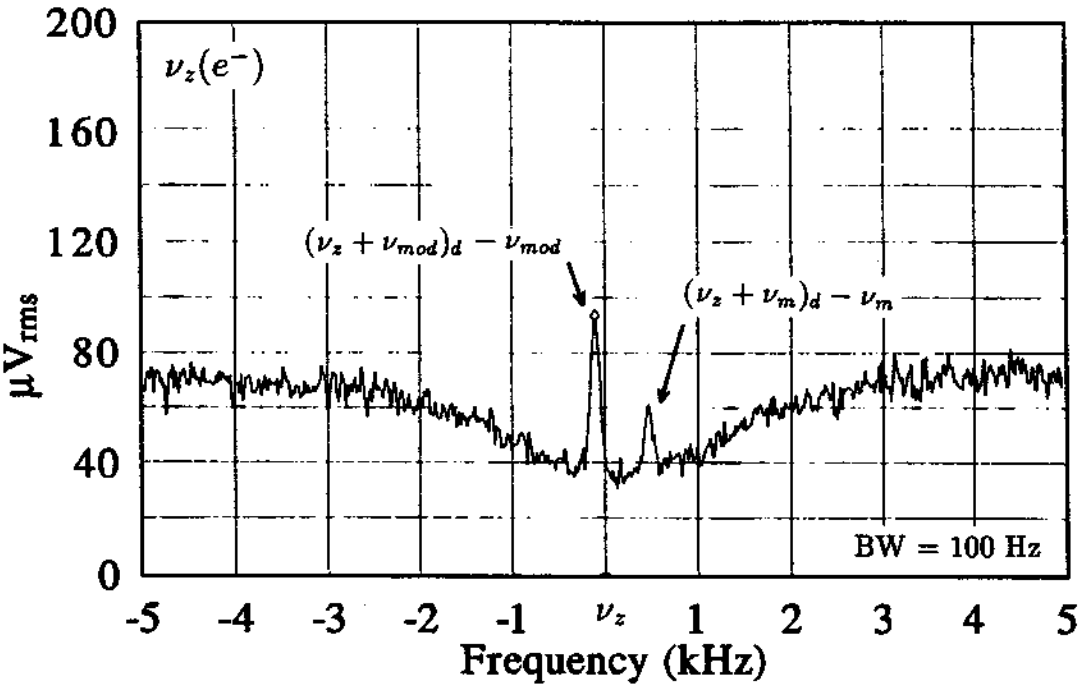

Figure 6.2: Locked axial electron responses to the axial and off resonant axial magnetron sideband drive.

The signal to noise obtainable using the lock correction signal depends on the circuit time constants and also on the application of magnetron sideband cooling. Sideband cooling insures that the electrons remain radially centered and oscillate in the optimally tuned region of the trap.

An artifact of the axial frequency being locked is that it can be simultaneously observed in the 'dip' in the noise spectra (Fig. 6.2). The response at ν_z is the electron response to a drive source at $(\nu_z + \nu_{mod})_d$ while the ring is modulated at ν_{mod}. The width of the response signal is extremely narrow (the width of the drive synthesizer) and is bandwidth limited in this figure. The other response in the figure is due to a magnetron sideband drive near $(\nu_z + \nu_m)_d$. This response (at $[(\nu_z + \nu_m)_d - \nu_m]$) where $(\nu_z + \nu_m)_d$ is approximately $\nu_z + \nu_m$ is interesting in two respects. First, the response at ν_z has no width except that due to the resolution of the analyzer. When the sideband response has an observable width, it can be used for the purpose of tuning the trap and to yield information on effects that may cause variations in ν_m . Second, a measurement of this sideband when subtracted from the cooling drive frequency yields a measure of the magnetron frequency. If $(\nu_z + \nu_m)_d$ is sufficiently strong, many sidebands can be directly observed.

6.1.3 Measurement of the Trap Orthogonalization

The coefficient D_2 (Chapter 3), which in a perfectly orthogonalized trap equals zero, can be determined by measuring the change in the axial frequency as a function of the trapping potentials V_0 and V_c by

$$\frac{D_2}{C_2} \approx \frac{\partial \nu_z / \partial V_c}{\partial \nu_z / \partial V_0}. \tag{6.5}$$

This is done by observing the shift of a narrow dip as a function of changing the trap potential, or by measuring the calibrated correction of the lock circuit due to tuning changes.

Though the parameters of the trap have not yet been measured with a single electron, measurements based on approximately 300 electrons yield a limit of

$$\frac{D_2}{C_2}(300\ e^-) \leq 8 \times 10^{-3}. \tag{6.6}$$

The degree of orthogonalization is observed to improve with decreasing particle number.

6.2 Detecting the Cyclotron Motion

The cyclotron motion ν_c' of electrons in a 5.9 T field is in the millimeter microwave regime at about 164 GHz, and is not accessible by direct detection. This motion, is instead measured by observing the axial signal as a function of cyclotron drive frequency. On resonance, energy is absorbed by the cyclotron motion, which can then couple to and be observed as small changes in the axial motion. The coupling mechanism can be by collisions, anharmonicity, magnetic gradients [101], or even special relativity [33].

6.2.1 Microwave Source

To excite the cyclotron motion of electrons requires a microwave source that can be swept over small regions near 164 GHz. To produce 164 GHz microwaves in the open endcap trap we have assembled a system schematically shown in Fig. 6.3. The fundamental frequency of 640 MHz is obtained from the fixed output of an HP 8662A frequency synthesizer and filtered with a copper cavity filter. The 640 MHz signal is amplified by +21.4 dB and put into an HP 33004A-H26 step recovery diode. The output goes through a filter at 10.240 GHz (bandpass = 0.275 GHz) which only passes the 16^{th} harmonic from the step recovery diode. The output is then amplified by 17 dB and sent through a WMI 8838 circulator to avoid reflections from the following mixer. The 10.24 GHz signal is then mixed with the variable output of the HP 8662A synthesizer. The mix frequency is about 700 MHz (amplitude $\approx$ -19 dBm). The mixed output is passed through a 10.94 GHz filter (bandpass 0.250 GHz) to select the high component. The 10.94 GHz output signal is amplified another 19 dB and then sent out of the RF cabin to the trap through an 8 meter long microwave transmission cable. The cable is measured to attenuate the 10.94 GHz signal by 13.2 dB. The signal is then amplified (to a maximum of +20 dBm) with an HP 8349B broadband amplifier. Before entering

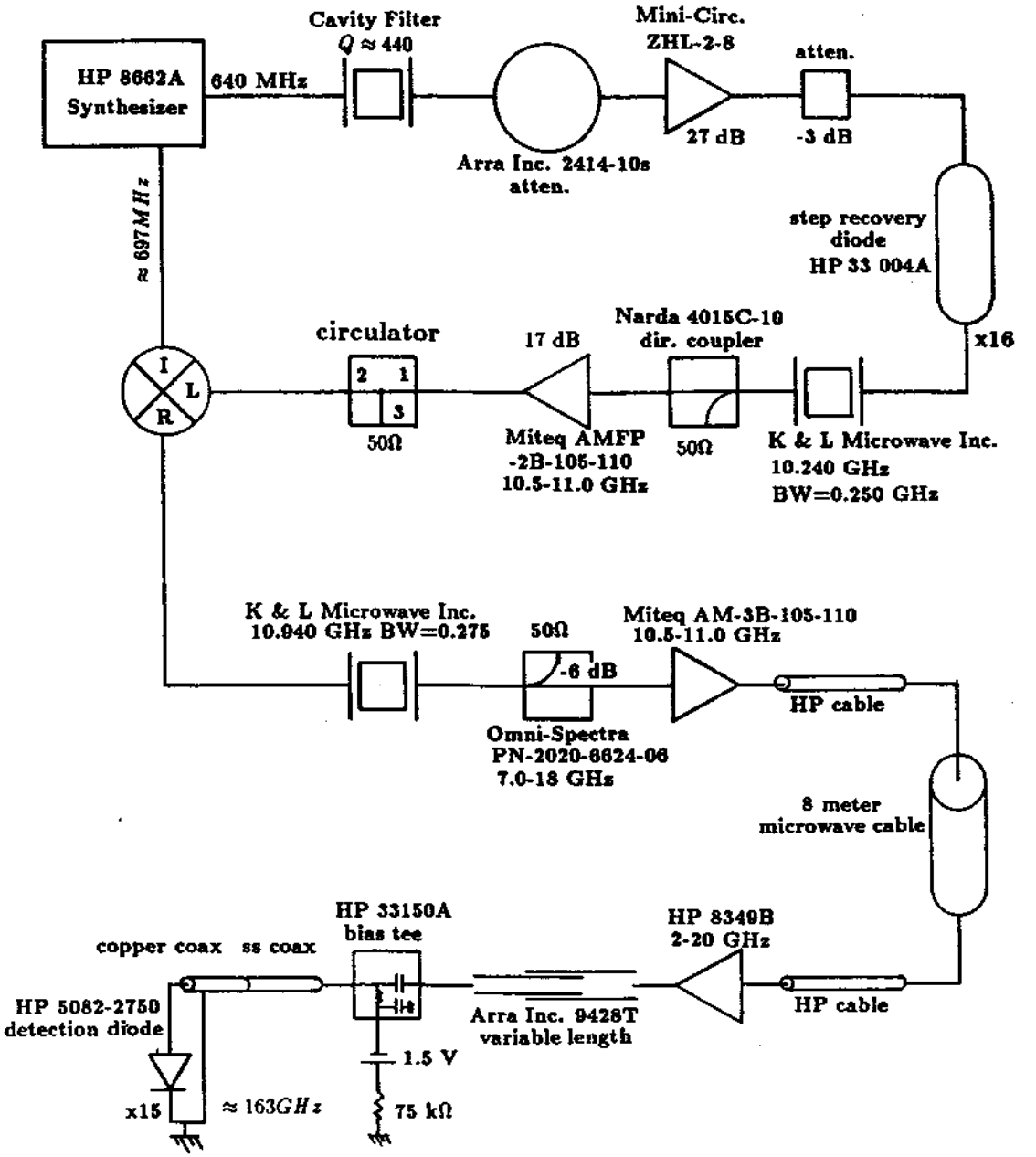

Figure 6.3: The microwave system used to excite the electron cyclotron motion at about 163 GHz.

the brass hat a variable length is included and the 10.94 GHz signal is coupled onto a dc bias line.

The signal enters the bore vacuum through a 50 Ω SMA feedthrough and travels down a 0.3 meter long, .050" diameter SS coaxial cable, then through a 0.7 meter long, .050" diameter copper coaxial cable. The coaxial cable is terminated with an HP 5082-2750 series detection diode which has a line of sight path to the trap center through a glass to metal seal in the trap vacuum enclosure (see Fig. 5.5).

The 10.94 GHz signal, which can be swept as wide as 0.25 GHz, drives the terminating detection diode. The cyclotron drive signal is the 15th harmonic given by

$$\nu_c'(e^-) = ((640 \times 16) + \nu_d) \times 15\ MHz \tag{6.7}$$

For a frequency input of $\nu_d = 700$ MHz, the diode produces a useful signal at 164.1 GHz with a possible range of 3.75 GHz or $\Delta\nu_c/\nu_c \approx 2\%$.

The diode is kept dc biased with a constant current of $I_{bias} = 20\mu$A. The minimum power on the diode necessary to excite the electron cyclotron frequency is about -3 dBm at 10.94 GHz.

6.2.2 Anharmonicity Coupling of ν_c' and ν_z

Techniques for detecting the cyclotron (or spin state) of an electron via small shifts in the locked axial frequency have been highly refined, particularly for measurements of the anomalous magnetic moment (or g-2) of the electron [101,13]. The coupling of the cyclotron or spin into the axial frequency has normally been accomplished with the inclusion of a magnetic gradient (an intentional magnetic bottle field) [25]. Such magnetic bottles lead to broad resonance lines and amplitude (power) dependent shifts that theoretical interpretation [9]. For mass spectroscopy at the level we report here, magnetic bottles are not necessary or desirable for detecting the electron cyclotron motion.

Without a magnetic bottle, the cyclotron resonance of a single electron can be detected using relativistic coupling [33]. However, at the precision reported here, there is no need to deal with only a single electron in the trap. Instead, we use small clouds consisting of $\approx 500 \rightarrow 2000$ electrons, and detect the excitation of

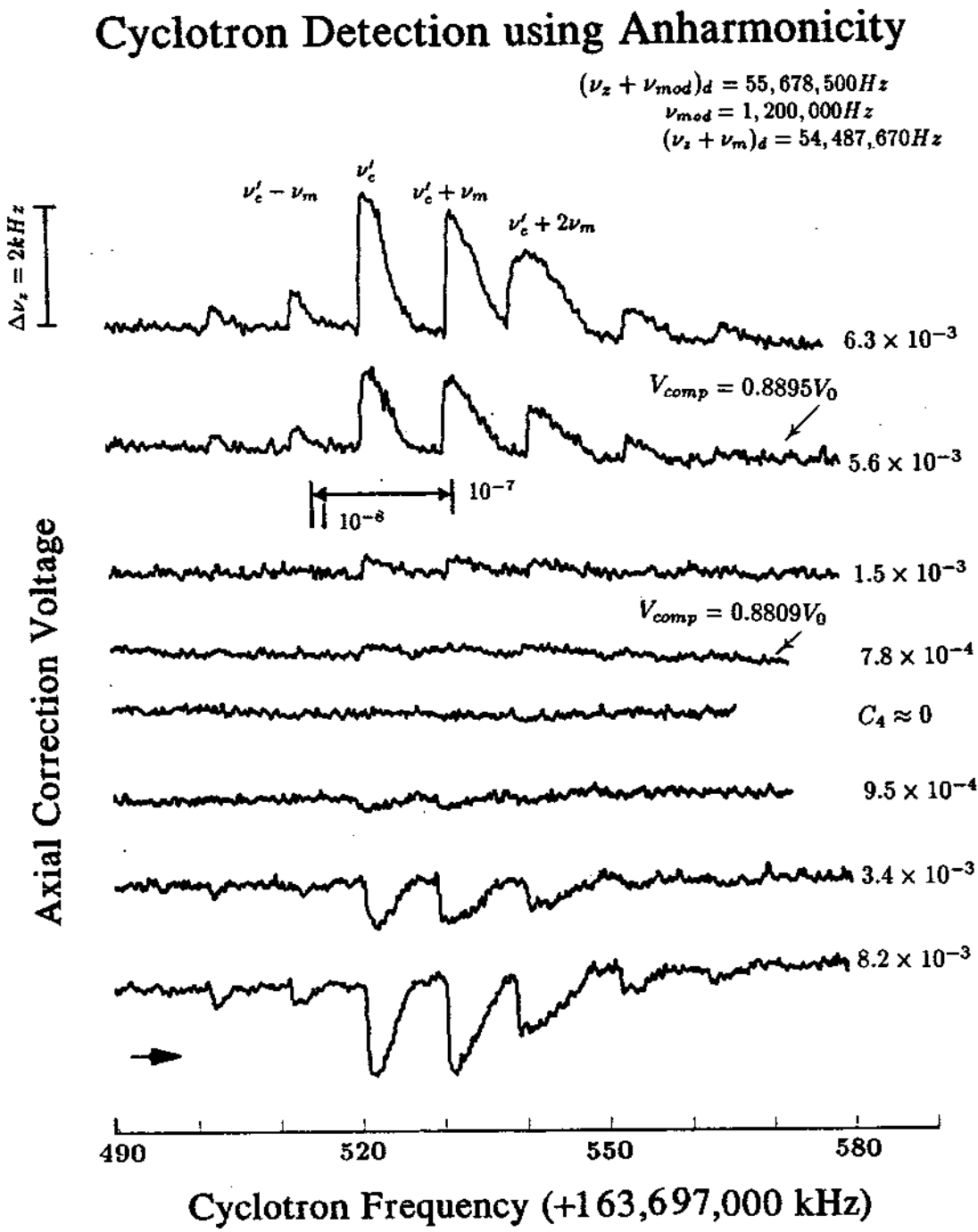

Figure 6.4: Locked axial feedback signal as a function of cyclotron drive frequency. Each trace corresponds to a different compensation setting V_{comp}/V_0. The applied microwave drive strength and sweep rate is constant for all traces.

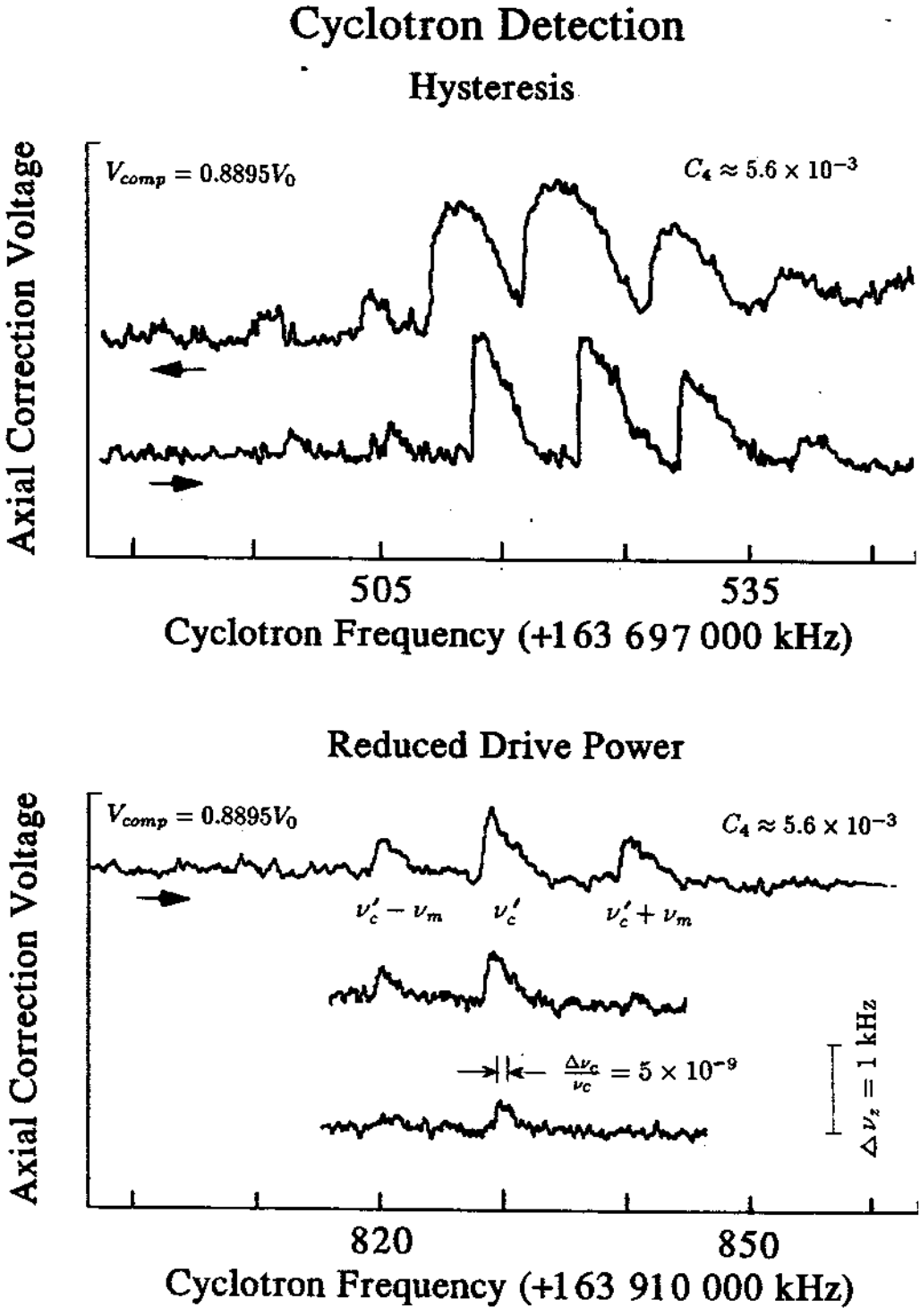

Figure 6.5: Cyclotron resonances as observed by monitoring the locked axial feedback signal as a function of cyclotron drive frequency. (a) Hysteresis depending upon sweep direction, and (b) effect of reducing microwave power to resolve on ν_c'.

ν_c' via the locked axial signal by intentionally introducing trap anharmonicity. The ability to do this is greatly enhanced by the orthogonalization of the trap.

The axial feedback signal as a function of microwave cyclotron excitation frequency is shown in Fig. 6.4. The correction signal (corresponding to $\Delta\nu_z$) depends on the degree of mistuning V_c/V_0 (i.e. an increase in the potential term proportional to C_4). The microwave drive amplitude, sweep rate, and direction are the same for all the traces shown. Several magnetron sidebands at $\nu_c' \pm k\nu_m$ (k=1,2,3...) are resolved as well as ν_c' .

For the trap tuned such that $C_4 \approx 0$ we observe little coupling of the cyclotron heating to the axial motion within the sensitivity of the detection. To see any perturbation on the locked axial signal for a tuned trap requires increasing the drive strength by more than 12 dB at 10.94 GHz. For the electron cyclotron measurements used in the mass comparison, we typically operate the trap with the compensation electrodes mistuned ($V_{comp} = 0.8895V_0, C_4 \approx 5.6 \times 10^{-3}$) so that less cyclotron heating is necessary to observe the coupling into the axial motion. In Fig. 6.4, we observe that changes in C_4 evidently does not shift the cyclotron frequency within the $5\times\ 10^{-9}$ resolution observable along the signal edge. The cyclotron motion is not very sensitive to the electostatic conditions of the trap, even though the axial frequency is very sensitive to changes in C_4.

In Fig. 6.5(a) we show frequency sweeps obtained using the same drive strengths and sweep rates in both directions. The signal shows a hysteretic behavior and resembles in many ways the anharmonic lineshapes commonly observed in axial lineshapes for a mistuned trap. While the shift in the axial frequency $\Delta\nu_z$ is clearly due to the inclusion of C_4, we do not see a change in the linewidth (i.e. $\Delta\nu_c'$) as a function of C_4 over the ranges of C_4 shown in Fig. 6.4.

In Fig. 6.5(b), we identify the modified cyclotron frequency ν_c' by reducing the microwave drive strength until it is the only one resolved. The total linewidth narrows as we reduce the drive strength and a resolution of better than 1 part in 10^8 is shown. It suffices to obtain the free space cyclotron from $\nu_c = \nu_c' + (\nu_z^2/2\nu_c')$ [8]. Because the measurements are done with the axial frequency locked, the correction term $\nu_z^2/2\nu_c'$ is determined to high accuracy and the measurement

is limited by our understanding of the cyclotron linewidth $\Delta\nu_c'$.

Cyclotron measurements of a few or more electrons need not be done using the locked phase sensitive detected signal. We can also observe such signals using a 'bolometric' observation technique [108] when phase information of the particle motion is difficult to attain. By observing the square law output over a region spanning the 'dip' shown for example in Fig. 6.1(b), cyclotron resonances can be observed using increased microwave drive strengths of about +10 dB at 10.94 GHz. (Related techniques will be extremely useful in the work with ions and antiprotons). The drawback is that more heat increases the possibility of undesirable systematic shifts.

6.3 Other Applications with Electrons

The experimental determination of the electron magnetic moment [101] is one of the most direct and precise tests to date of quantum electrodynamics. Such measurements are typically performed with a single electron residing in a hyperbolic trap. The observation of the inhibition of the radiative decay of the electron in the radiation field in the cavity formed by the trap electrodes has raised the possibility that there may exist shifts in the measured electron cyclotron and spin frequencies [34] . Since the existence of cavity modes may have important consequences for the high precision g-2 measurements, much effort has gone into understanding and quantifying the modes of several trap geometries.

Some indications of modes in one hyperbolic trap have been observed [103] though there appears to be no correlation with calculated modes in such a trap [12]. Because of the difficulties in calculating the modes of a hyperbolic cavity, much effort has gone into quantifying the cyclotron motion of the electron in microwave cavities with simpler cylindrical [11] and spherical [14] geometries. Recently, a single electron has been observed in a cylindrical trap with flat endcaps [88] and modes with excellent signal to noise have been observed with a new technique [89].

The two approaches to removing the potential cavity perturbation from influencing high precision electron measurements are to either do the measurement

in a trap where the modes are known and quantified, or to build a trap which does not easily support modes. The open endcap cylindrical trap may provide an environment free of cavity modes. Because the endcaps are open cylinders, any standing wave mode that exists in the trapping region should be very weak. The open endcap Penning trap developed here for use with high energy antiprotons may have advantageous applications in the g-2 measurement of the electron.